

ACCEPTED MANUSCRIPT

Hot corrosion studies on fully austenitic stainless steel in air oxidation and simulated waste heat incinerator environment at 600 °C, 650 °C and 700°C

To cite this article before publication: Roshith P *et al* 2019 *Mater. Res. Express* in press <https://doi.org/10.1088/2053-1591/ab61ab>

Manuscript version: Accepted Manuscript

Accepted Manuscript is “the version of the article accepted for publication including all changes made as a result of the peer review process, and which may also include the addition to the article by IOP Publishing of a header, an article ID, a cover sheet and/or an ‘Accepted Manuscript’ watermark, but excluding any other editing, typesetting or other changes made by IOP Publishing and/or its licensors”

This Accepted Manuscript is © 2019 IOP Publishing Ltd.

During the embargo period (the 12 month period from the publication of the Version of Record of this article), the Accepted Manuscript is fully protected by copyright and cannot be reused or reposted elsewhere.

As the Version of Record of this article is going to be / has been published on a subscription basis, this Accepted Manuscript is available for reuse under a CC BY-NC-ND 3.0 licence after the 12 month embargo period.

After the embargo period, everyone is permitted to use copy and redistribute this article for non-commercial purposes only, provided that they adhere to all the terms of the licence <https://creativecommons.org/licenses/by-nc-nd/3.0>

Although reasonable endeavours have been taken to obtain all necessary permissions from third parties to include their copyrighted content within this article, their full citation and copyright line may not be present in this Accepted Manuscript version. Before using any content from this article, please refer to the Version of Record on IOPscience once published for full citation and copyright details, as permissions will likely be required. All third party content is fully copyright protected, unless specifically stated otherwise in the figure caption in the Version of Record.

View the [article online](#) for updates and enhancements.

Hot corrosion studies on fully austenitic stainless steel in air oxidation and simulated waste heat incinerator environment at 600 °C, 650 °C and 700°C

Roshith P^a, Arivarasu M^{b*}

^aSchool of Mechanical Engineering, Vellore Institute of Technology, Vellore, India

^bCentre for Innovative Manufacturing Research, Vellore Institute of Technology, Vellore, India

*arivarasu.m@vit.ac.in; arivarasu.m@gmail.com

Abstract

The purpose of the current study is to compare the hot corrosion performance of SMO 254 exposed to air oxidation and molten salt with a eutectic mixture of 40 wt.% Na₂SO₄ +40 wt.% K₂SO₄ +10 wt.% NaCl + 10 wt.% KCl at 600 °C , 650 °C and 700°C under cyclic conditions for 50 hours period. Kinetics of corrosion were analyzed by thermogravimetric method. By using SEM/EDS, the hot corroded specimens were investigated for surface scales and cross-sectional elemental analysis by point, line mapping methods. An accelerated rate of corrosion rate was noticed in the specimen exposed to molten salt at 700 °C, and the lowest rate of corrosion rate was observed in the specimen subjected to air oxidation at 600°C. XRD analysis is done to analyze the corrosion products in the oxide scale.

Keywords: Hot corrosion, Thermogravimetric chart, SEM/EDAX method, XRD analysis, air oxidation, Molten salt hot corrosion

1 Introduction

SMO 254 is widely used in the fields such as petrochemical, desalination, flue gas desulphurization, power generation, seawater piping, wastage incineration plants, and pharmaceutical plant due to its remarkable resistance to crevice and pitting corrosion [1-8].

Sanaa et al.[7] studied about the susceptibility of 254 SMO alloys to Crevice Corrosion in NaCl Solution. The author reported that the oxides of Cr, Fe and Mo formed during the crevice corrosion protects\gives resistance to the alloy against the crevice.

Meguid et al.[9] investigated the critical crevice potential and the critical protection potential for Alloy 254 using potentiodynamic cyclic anodic polarization technique. The author reported that SMO 254 was resistant to pitting and crevice in 4% NaCl solution till 90 °C.

1
2
3 Katiki et al.[10] indicated that the when the salts like K_2SO_4 , Na_2SO_4 , KCl , and $NaCl$ are
4 combined, their melting point falls well below the actual melting point of the salts, resulting in salt
5 fluxing causing destruction of the protective oxide layer triggering corrosion. The main governing
6 factors which affect high-temperature corrosion are salt mixture composition, coverage of
7 temperature, cyclic heating and cooling, and environmental conditions[11]. Hot corrosion is the
8 main issue faced in the petrochemical sections, industrial waste incinerators and power plant parts
9 such as boilers, internal combustion engines, etc [12]. Author Sidhu T.S et al.[13] observed that hot
10 corrosion cause reduction in the quantity of material and reduction in the load-bearing capabilities,
11 and finally it turns to catastrophic failure.
12
13
14
15
16
17
18

19 It has been found that from a thorough literature survey, the authors have studied the pitting and
20 crevice corrosion on SMO 254. However, though this SMO254 is a candidate material for the high-
21 temperature applications in the waste incinerator and power generation no detailed studies were
22 done on hot corrosion study. The experimental goal of this research work is to investigate the
23 behaviour of SMO 254 in hot corrosion environment in the simulated industrial waste incinerators
24 and the power plant environment. A comparative study on the air oxidation and hot corrosion
25 behaviour in the molten salt eutectic mixture of 40 wt.% Na_2SO_4 + 40 wt.% K_2SO_4 + 10 wt.%
26 $NaCl$ + 10 wt.% KCl at 600 °C , 650 °C and 700°C under cyclic conditions is carried out. To
27 derive the corrosion mechanism by a detailed study using the thermogravimetric analysis, surface
28 and cross- sectional analysis using SEM/EDS was done. Also, an attempt is made to identify the
29 corrosion products using EDS along with the SEM/EDS elemental analysis.
30
31
32
33
34
35
36
37
38
39
40

41 **2. Material and experimental procedure**

42 The material SMO 254 was purchased in the plate form from a reputed supplier. The chemical
43 composition of SMO254 is provided in **Table 1**. The base metal was cut in a dimension of 20 mm
44 length 10 mm width and 6 mm thickness. To maintain the uniform surface finish to avoid the effect
45 of surface roughness in the results the samples were polished. Standard procedure was followed
46 using silicon carbide emery papers in the order of 240,400,600,800,1000,1200,1500 and 2000 grits
47 followed by alumina slurry disc polishing. Finally, specimens were cleaned with warm water and
48 acetone. By using a vernier caliper surface area of the specimens was measured and weight was
49
50
51
52
53
54
55

1
2
3 measured by electronic balance with an accuracy of 0.01 mg. Three specimen were coated with 40
4 wt.% Na_2SO_4 + 40 wt.% K_2SO_4 +10 wt.% NaCl +10 wt.% KCl salt by using camel brush. The
5 salts were applied to the specimen only during the initial stage. The weight of coated salt varies
6 from 3 mg/cm^2 to 5 mg/cm^2 . The alumina boats were annealed at a temperature of 1200 °C for 24
7 hours. Before the hot corrosion studies, specimens were dried in the alumina boats at 200°C for 2
8 hours to remove moisture content. The experiments were carried out in three different tubular
9 furnaces with the heating system precision of (+2°C to -2°C). Both oxidation and hot corrosion
10 were conducted at three different temperatures 600, 650 and 700 up to 5 cycles. Each cycle
11 involves 10 hours heating followed by 20 minutes cooling at room temperature. After completing
12 each cycle weight of specimens along with the boat was measured accurately to find the weight
13 gain\loss corrosion. Proper visual surveillance was made to understand the spalling, sputtering and
14 colour changes of the oxides.
15
16
17
18
19
20
21
22
23

24 **3. Results and Discussion**

25 *3.1 kinetics of corrosion*

26
27
28
29 The thermogravimetric charts of the different specimens after air oxidation and hot corrosion is
30 given in Figure 1(a & b). The images of the specimens after and before air oxidation and hot
31 corrosion are given in Figure (2&3).
32
33
34

35 It is noted that from the macro images at the end of the first cycle(after 10 hours) in the air
36 oxidized samples the colour of specimen turned to reddish- brown at 600 and 650 °C. However, in
37 the case of 700 °C it turned in to bluish- black. The hot corroded samples turned to black, however
38 without any spalling of oxide scales.
39
40
41
42

43 At the end of 20 hours spalling was observed in the specimen subjected to hot corrosion at 700°C
44 with the other samples in air oxidization and hot corrosion remained unaffected suggesting that the
45 corrosion rate of the hot corroded sample is accelerating,
46
47

48 At the end of the 5th cycle, it is observed that specimen which is exposed at molten salt at 700 °C
49 showed a higher rate of corrosion rate than others. The specimen exposed to air oxidation at 600 °C
50 suffered the lowest rate of corrosion. The parabolic law of oxidation was followed by all the
51
52
53
54
55
56
57
58
59
60

samples in both environments. The equation which is used to find the parabolic rate (K_p) is given bellows [11].

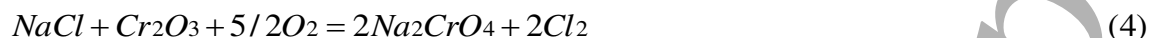
$$\left(\frac{\Delta W}{A}\right)^2 = K_p \times t \quad (1)$$

Where, ΔW is the variation in the substrate weight with respect to the initial weight. 't' is the time of oxidation in seconds. Here the unit area is indicated by symbol "A" The K_p value of all substrates is given in Table 2. Author Nakagawa K et al.[14] reported that the eutectic temperature of the molten salt composition is 520°C. From **Table 2**, it is observed that the total weight gain is higher for specimens exposed to molten salt corrosion at 700°C and a comparatively lower amount of weight gain for specimens exposed to air oxidation at 600°C. The samples subjected to air oxidation received lower weight gain than the specimen exposed to the molten salt environment. Also, a higher value of K_p is obtained for the specimen exposed to molten salt corrosion at 700°C, and the lower value of K_p is obtained for the specimen exposed to air oxidation at 600°C.

3.2 SEM/EDAX analysis

Surface SEM images of the hot corroded specimens are provided in Figure 4 (a-f). SEM images indicate that formation of the coarse uneven surface. On close observation of the specimen, micropores are noticed on the top surface. Also, micro-cracks are observed in Figure 4 (b & f). Volatile chlorides diffuse out the surface through these micro-cracks. Cross-sectional SEM images with point analysis, line mapping are represented in Figures (5-10). EDS results imply that the scales mainly include oxides of elements such as Cr, Fe, and Ni. It can be noted that the results produced in the EDS report are closer to that of XRD data. Author Muthu S et al.[15] reported that NaCl salt is vigorous at the higher temperature. Hence it can create pores in the surface also Cl in the salt react with metal substrate and form corrosive corrosion products such as $ClCo_2O_4P$, $ClCrKO_3$, $ClCu$, $ClCuFe_{24}K_6S$, $ClCu_2O_3$, ClK , $ClCu_{4.37}Na_4$ and $ClNa$ which are evaporative and porous owe to greater vapour pressure and low melting point. Arivarasu et al. mentioned that these metallic chlorides with O_2 create the non-protective oxide layers with porous structure [11]. The chlorine is discharged due to the sulphation of chloride enclosing deposits [16].





Also, the sodium sulphate present in the molten salt dissociates as per the following reaction.



The above Na_2SO_4 dissociation mechanism can be explained based on the lewis acid-base concept, where initially formed component Na_2O is a basic part, and SO_3 is acidic. It is clear that SO_3 is in stable condition with oxygen and sulphur. So it can be concluded that when O_2 partial pressure drops, the increment in the partial pressure of S_2 occurs. This result improvement of the partial pressure of S_2 in the molten salt, when the absorption of O_2 has occurred.

The S_2 in the Na_2SO_4 migrate into the base metal and cause degradation of the base metal by increasing the oxidation rate. Which indicates the rapid weight gain the molten salt coated specimen. Cross-sectional SEM images with EDS results of the specimen exposed to air oxidation at 600 °C after 5 cycles is given in Figure 5a. On analyzing Figure 5a it can be noted that a higher amount of O_2 in location 1 with weight % of 38.95 and lack of oxygen creation was noted in the location 2,3 & 4. In location 1 it is observed that lower weight % of Cr (5.01) and higher quantity of Mo with a weight % of 42.42. Cross-sectional line mapping images of the specimen exposed to air oxidation at 600 °C after 5 cycles are provided in Figure 5b. Cross-sectional SEM images with EDS results of the specimen exposed to molten salt at 600 °C after 5 cycles are given in Figure 6a. While analyzing Figure 6a it can understand that higher concentration of O_2 is observed in location 1 (weight % of 12.55) and lower weight % of O_2 in location 3 (weight % of 2.61). Cross-sectional line mapping of the specimen exposed to molten salt at 600 °C after 5 cycles is provided in Figure 6 (b). Corrosive nature having Silicon is present in location 3 with 4.61 weight%. Cr and Mo weight % improves in both position 1&2. Cross-sectional SEM images with EDS results of the specimen exposed to air oxidation at 650 °C after 5 cycles is given in Figure 7a, and it can be identified that higher concentration of O_2 at position 1 with a weight % of 27.65 and lower weight of O_2 (3.80) in location 2. Also, it is witnessed that the improved rate of Cr in all positions (1-3). Nickel quantity is

1
2
3 reduced in both positions 1 & 2, also slight increments of concentration in both 3 & 4 locations.
4 Corrosive element sulfur is present in location 3 with a weight % of 2.27. Cross-sectional line
5 mapping of the specimen exposed to air oxidation at 650 °C after 5 cycles is given in Figure 7 (b).
6 Cross-sectional SEM images with EDS results of the specimen exposed to molten salt at 650 °C
7 after 5 cycles is provided in Figure 8a and while analyzing it can be observed that a higher
8 concentration of O₂ in all positions (1-4) with a concentration of (27.58 %, 11.60%, 6.39% and
9 7.86%). Also, corrosive nature having element Sulphur is present in location 1 & 3 with a
10 concentration of 0.58 % and 3.94%. A higher rate of Cr is observed in all four positions with a
11 concentration of 24%, 27%, 22.81%, and 23.20%. Cross-sectional line mapping of the specimen
12 exposed to molten salt at 650 °C after 5 cycles is given in Figure 8 (b). Cross-sectional SEM images
13 with EDS results of the specimen exposed to air oxidation at 700 °C after 5 cycles is given in
14 Figure 9a and the EDAX image indicates that higher concentration of O₂ in position 1 with a
15 weight % of 14.81 and reduced quantity of O₂ is observed in the location 4 with a weight % of 1.41.
16 Also, it is noted that a slightly improved rate in the quantity of Ni in location 2,3 & 4. Cross-
17 sectional line mapping of the specimen exposed to air oxidation at 700 °C after 5 cycles is given in
18 Figure 9 (b). Cross-sectional SEM images with EDS results of the specimen exposed to molten salt
19 at 700 °C after 5 cycles is given in Figure 10a. Augmented rate of O₂ is observed in Figure 10a at
20 location 2 with a weight % of 30.96, and increment in the rate of Mo is observed in location 1&2
21 with a concentration of 9.67 % & 28.85 %. Also, corrosive nature having element sodium is
22 observed in location 2 with a weight % of 4.72. Cross-sectional line mapping of the specimen
23 exposed to molten salt at 700 °C after 5 cycles is given in Figure 10 (b).
24
25
26
27
28
29
30
31
32
33
34
35
36
37
38
39

40 3.3 XRD analysis

41
42 By using D8 Advanced Brunker (Germany), XRD analysis was carried out. XRD pattern of the
43 specimens is given in Figure 11. The corrosion products formed during air oxidation at 600 °C are
44 FeNi, Ni₃Si, Cr_{0.4}Ni_{0.6}, Ni₃P₂, CuNi, Co_{0.9}Mo_{0.1}, Mo_{0.9}Ni_{0.91} and Co_{0.027}Fe_{0.2}. And the corrosion
45 products formed during molten salt hot corrosion at 600 °C are ClCu₂O₄P, ClCrKO₃, ClCu,
46 ClCuFe₂₄K₆S, ClCu₂O₃, ClK, ClCu_{4.37}Na₄ and ClNa. The corrosion products such as Fe_{0.8}Mn_{0.2},
47 Ni₃Si, MnSi, Co_{0.027}Fe_{0.2}, CrNi₃, CuNi, Mo_{0.09}Ni_{0.91}, and FeNi₃ are produced after air oxidation for
48 50 hours at 650 °C. Also, the formation of corrosion products such as ClCuFe₂₄K₆S, ClFe₂₄K₆S₂₆,
49 ClK, ClK_{0.1}Na_{0.9}, ClNa, Cl₁₀MO₂ was observed after molten salt corrosion for 50 hours at 650 °C.
50
51
52
53
54
55
56
57
58
59
60

The corrosion products obtained after air oxidation for 50 hours at 700 °C are FeNi₃, Ni₃Si, Co_{0.027}Fe_{0.2}, MnSi, Co_{0.85}SiO_{0.15}, and Cr₃Si. Also, the corrosion products formed after molten salt hot corrosion for 50 hours at 700 °C are Co_{0.027}Fe_{0.2}, CrNi₃, Co_{0.85}SiO_{0.15}, MnS, FeNi₃, Ni₃Si, CrFe, Cu₂S, and Fe_{0.8}Mn_{0.2}. This data implies that the formation of beneficial corrosion products helped to stay with reduced corrosion rate on the specimen, which was undergone hot corrosion at 600 °C while comparing with the specimen exposed at the augmented temperature level.

Conclusion

1. It can be concluded that overall the hot corrosion is severe compared to oxidation in all the cases, and the severity of hot corrosion at 700 °C is 74.75% times than the hot corrosion at 600°C suggesting the effect of temperature.
2. The rate of corrosion in the below- mentioned order
Molten salt corrosion at 700 °C > air oxidation at 700 °C > molten salt corrosion at 650 °C > air oxidation at 650 °C > molten salt corrosion at 600 °C > air oxidation at 600 °C
3. SEM/EDS and XRD analysis have indicated the creation of corrosion products such as FeNi, Cr_{0.4}Ni_{0.6}, Ni₅P₂, Mo_{0.9}Ni_{0.91}, and CrNi₃ helped to increase corrosion resistance and MnS, Cu₂S caused reduction of hot corrosion resistance.
4. Formation of spinal oxides Mo_{0.09}Ni_{0.91}, Co_{0.85}SiO_{0.15}, oxide phases provide excellent resistance to corrosion of substrates.
5. Owe to the thermal stress, minor spallation has occurred in the specimen, which is exposed to molten salt corrosion and air oxidation at 700 °C.

Acknowledgment

Authors would like to thank VIT management for facilitating VIT SEED GRANT to purchase SMO 254 plates, and we wish to show gratitude to Prof. U. Narendra Kumar, for providing hot corrosion test facilities at Materials Engineering Laboratory at VIT.

References

- [1]. Roshith P, Arivarasu M, Arivazhagan N, Srinivasan A, KV PP. Investigations on induced residual stresses, mechanical and metallurgical properties of CO₂ laser beam, and pulse current gas tungsten arc welded SMO 254. Journal of Manufacturing Processes. 2019 Aug 1;44:81-90.

- 1
2
3 [2]. Hill R, Perez AL. New steels and corrosion-resistant alloys. In Trends in Oil and Gas
4 Corrosion Research and Technologies 2017 Jan 1 (pp. 613-626). Woodhead Publishing.
5 [3]. Khanna AS. 9 selection of materials for corrosion and materials in the oil and gas industries
6 Vol.3. 2016.p.197.
7 [4]. Rajala P, Bomberg M, Huttunen-Saarivirta E, Priha O, Tausa M, Carpén L. Influence of
8 chlorination and choice of materials on fouling in cooling water system under brackish
9 seawater conditions. Materials 2016;9(6):475.
10 [5]. Bingham RV, Nuttall D. EUROCORR 2017 in combination with the 20th international
11 corrosion Congress and the process safety congress 2017: corrosion control for safer living.
12 Part 2. Corros Eng Sci Technol 2018;53(3):163–72.
13 [6]. Zelenskiy VV, Nesterenko SV, Bannikov LP. Corrosion resistance of nickel steel and nickel
14 alloys in aggressive media. Coke Chem 2014;57(4):167–76.
15 [7]. Arab ST, Abdulsalam MI, Alghamdi HM. Susceptibility of 254 SMO alloys to crevice
16 corrosion in NaCl solution. Arab J Sci Eng 2014;39(7):5405–12.
17 [8]. Hao YS, Liu WC, Liu ZY. Microstructure evolution and strain-dependent constitutive
18 modeling to predict the flow behavior of 20Cr–24Ni–6Mo super-austenitic stainless steel
19 during hot deformation. Acta Metall Sin (English Letters) 2018;31(4):401–14.
20 [9]. El Meguid EA, El Latif AA. Electrochemical and SEM study on Type 254 SMO stainless
21 steel in chloride solutions. Corrosion science. 2004 Oct 1;46(10):2431-44.
22 [10]. Katiki, K., Yadlapati, S., Chidepudi, S.N.S., Manikandan, M., Arivarasu, M., Devendranath
23 Ramkumar, K. and Arivazhagan, N., Characterization of oxide scales to evaluate hot
24 corrosion behavior of ZrO₂ and Al₂O₃-TiO₂ plasma sprayed superalloy.
25 [11]. Arivarasu M, Venkatesh Kannan M, Devendranath Ramkumar K, Arivazhagan N. Hot-
26 corrosion resistance of dissimilar AISI 4340 and AISI 304L weldments in the molten salt
27 environment at 600° C. Corrosion Engineering, Science and Technology. 2017 Feb
28 17;52(2):114-23..
29 [12]. Eliaz N, Shemesh G, Latanision RM. Hot corrosion in gas turbine components. Engineering
30 failure analysis. 2002 Feb 1;9(1):31-43.
31 [13]. Sidhu, T.S., Malik, A., Prakash, S. and Agrawal, R.D., 2007. Oxidation and hot corrosion
32 resistance of HVOF WC-NiCrFeSiB coating on Ni- and Fe-based superalloys at 800
33 C. *Journal of Thermal Spray Technology*, 16(5-6), pp.844-849.
34 [14]. Nakagawa K, Matsunaga Y. The effect of chemical composition of ash deposit on the
35 corrosion of boiler tubes in waste incinerators. In Materials science forum 1997 (Vol. 251,
36 pp. 535-542). Trans Tech Publications.
37 [15]. Muthu, S.M. and Arivarasu, M., Air Oxidation and Hot Corrosion Behavior of Bare and CO
38 2 Laser-Welded Superalloy A-286 at 700° C. *Transactions of the Indian Institute of Metals*,
39 pp.1-6.
40 [16]. Grabke HJ, Reese E, Spiegel M. The effects of chlorides, hydrogen chloride, and sulfur
41 dioxide in the oxidation of steels below deposits. Corrosion science. 1995 Jul 1;37(7):1023-
42 43.
43
44
45
46
47
48
49
50
51
52
53
54
55
56
57
58
59
60

Table 1. Chemical composition of the base metal.

Fe	Cr	Ni	Mo	Mn	Nb	Ta	C	Others
55.16	19.61	17.59	6.17	0.36	-	-	0.01	Si-0.21; P-0.01; S-0.003; N-0.186; Cu-0.366; Co-0.07; Nb- 0.0069; V-0.016; W-0.011

Table 2. Weight gain, oxidation and hot corrosion kinetic of specimens.

Specimen	Total weight gain (mg/cm ²)	K _p (g ² /cm ⁴ /s ⁻¹)
Air oxidation at 600°C	0.19170132	2.041633116×10 ⁽⁻⁷⁾
Molten salt at 600°C	0.39170132	8.523884672×10 ⁽⁻⁷⁾
Air oxidation at 650°C	0.476581323	1.26183196×10 ⁽⁻⁶⁾
Molten salt at 650°C	0.547806103	1.667175147×10 ⁽⁻⁶⁾
Air oxidation at 700°C	0.583657588	1.892534334×10 ⁽⁻⁶⁾
Molten salt at 700°C	0.684565489	2.603499493×10 ⁽⁻⁶⁾

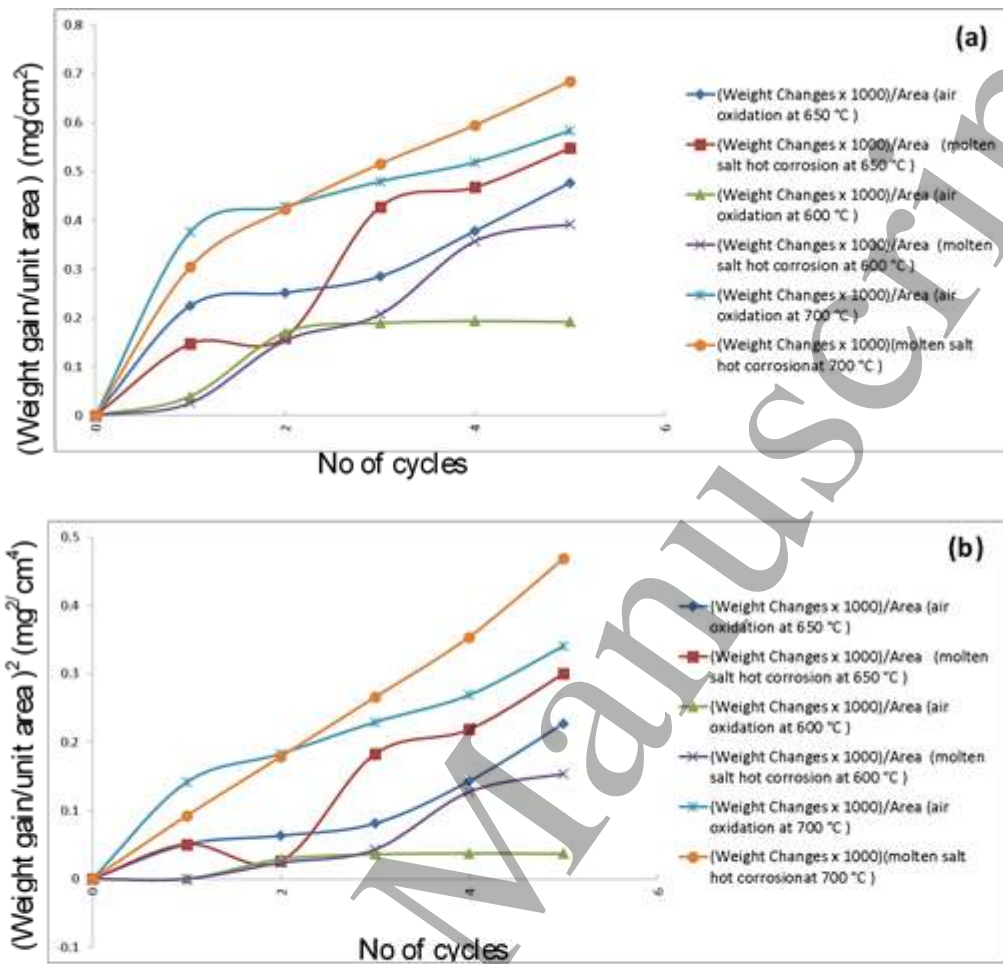


Figure 1: Thermo gravimetric analysis of air-oxidized and hot-corroded specimens.(a) Weight gain/area versus number of cycles, (b) weight gain/area² versus number of cycle.

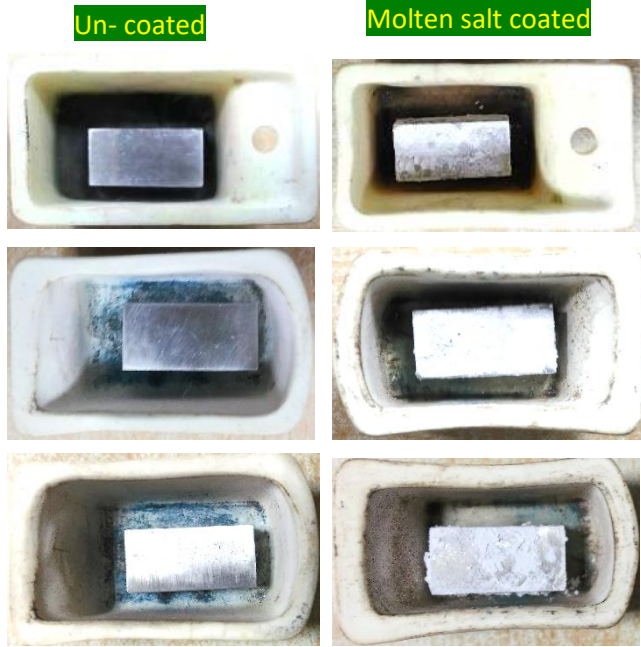


Figure 2: Images of specimen before hot corrosion

Accepted Manuscript

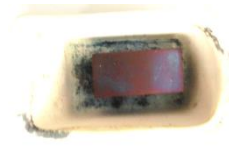
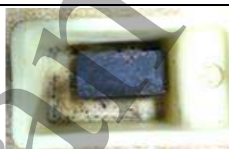
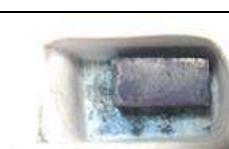
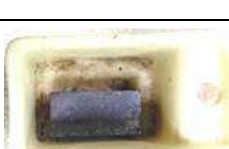
Cycle		600 ° C	650 ° C	700 ° C
1 st Cycle (10 Hours)	Air oxidized			
	Hot corroded			
2 st Cycle (20 Hours)	Air oxidized			
	Hot corroded			
3 st Cycle (30 Hours)	Air oxidized			
	Hot corroded			
4 st Cycle (40 Hours)	Air oxidized			
	Hot corroded			
5 th Cycle (50 Hours)	Air oxidized			



Figure 3: Macrographic images showing the air oxidized and hot corroded samples at the end of 10,20,30,40 and 50 hours

Accepted Manuscript

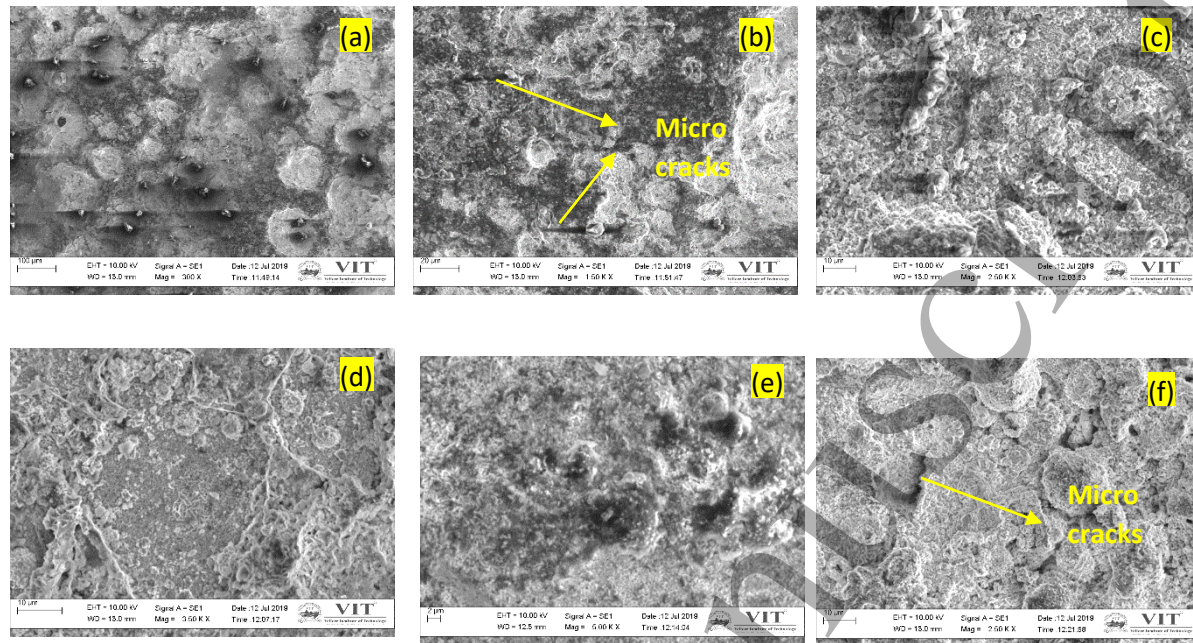
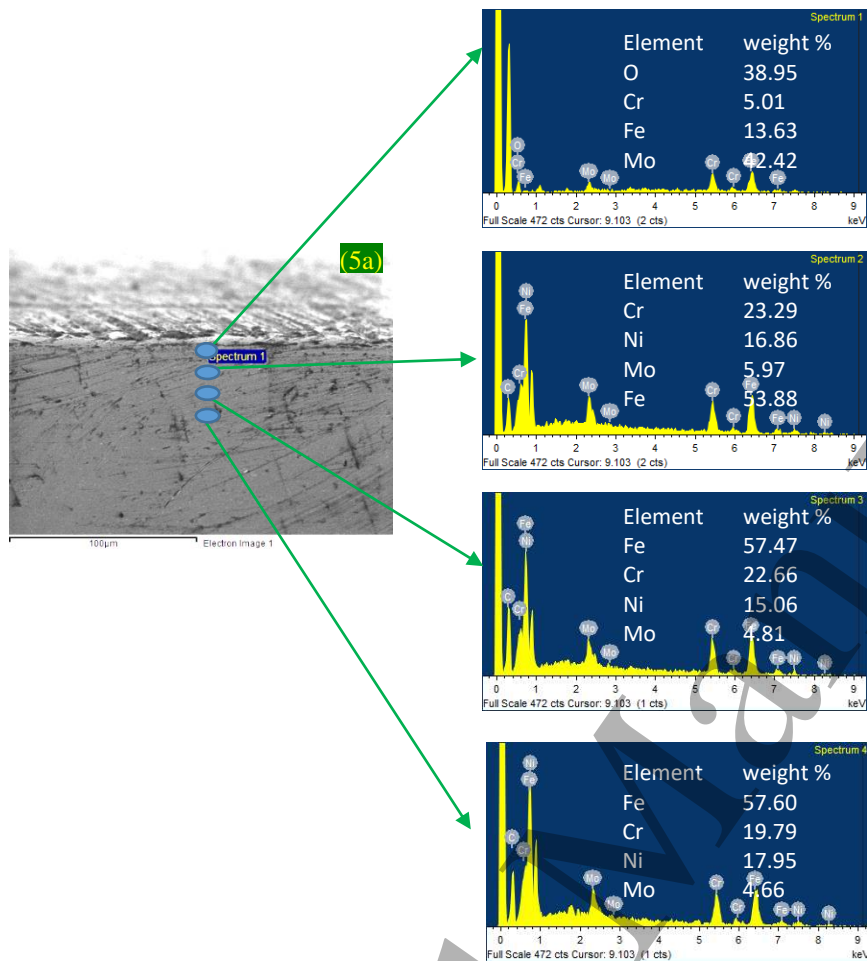


Figure 4: Surface SEM images of the specimen after 5th cycle

- (a) specimen after air oxidation at 600 °C (b) specimen after molten salt corrosion at 600 °C
(c) specimen after air oxidation at 650 °C (d) specimen after molten salt corrosion at 650 °C
(e) specimen after air oxidation at 700 °C (f) specimen after molten salt corrosion at 700 °C



34 **Figure 5a:** Cross -sectional SEM images with EDS results of the specimen exposed to air oxidation at 600 °C
 35 after 5 cycles.
 36
 37
 38
 39
 40
 41
 42
 43
 44
 45
 46
 47
 48
 49
 50
 51
 52
 53
 54
 55
 56
 57
 58
 59
 60

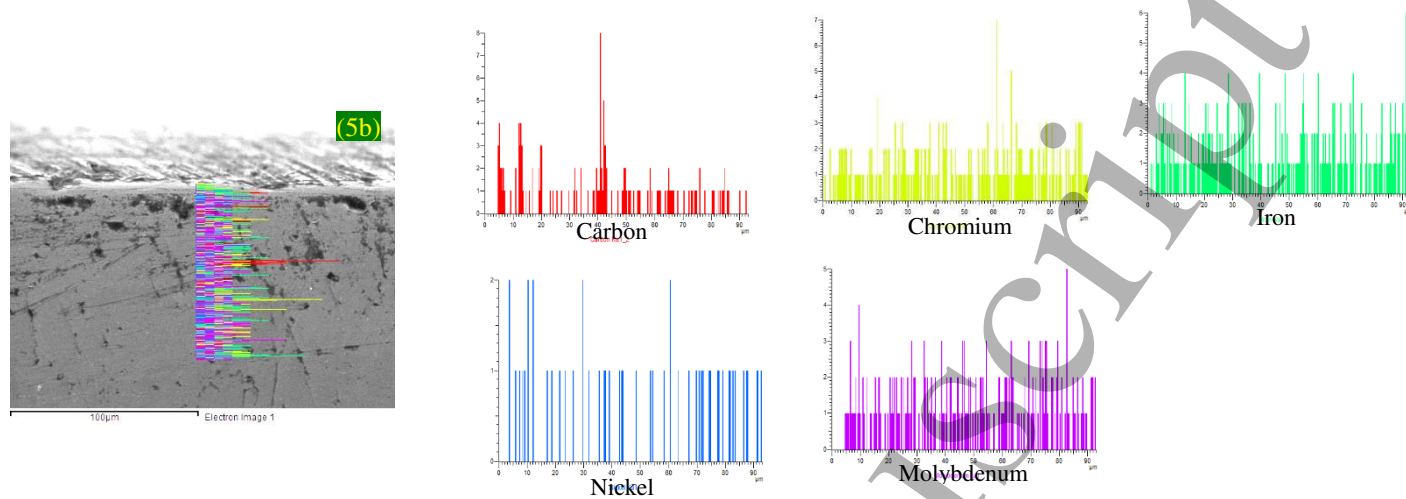
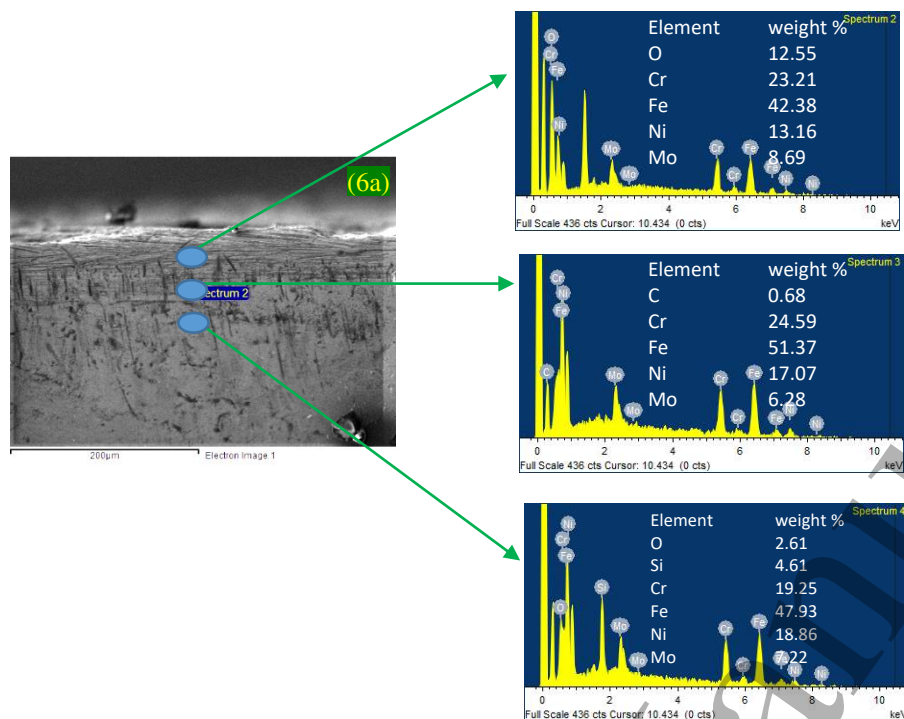


Figure 5b: Cross-sectional line mapping images of the specimen exposed to air oxidation at 600 °C after 5 cycles.



27 **Figure 6a:** Cross- sectional SEM images with EDS results of the specimen exposed to molten salt at 600 °C
28 after 5 cycles.
29
30
31
32
33
34
35
36
37
38
39
40
41
42
43
44
45
46
47
48
49
50
51
52
53
54
55
56
57
58
59
60

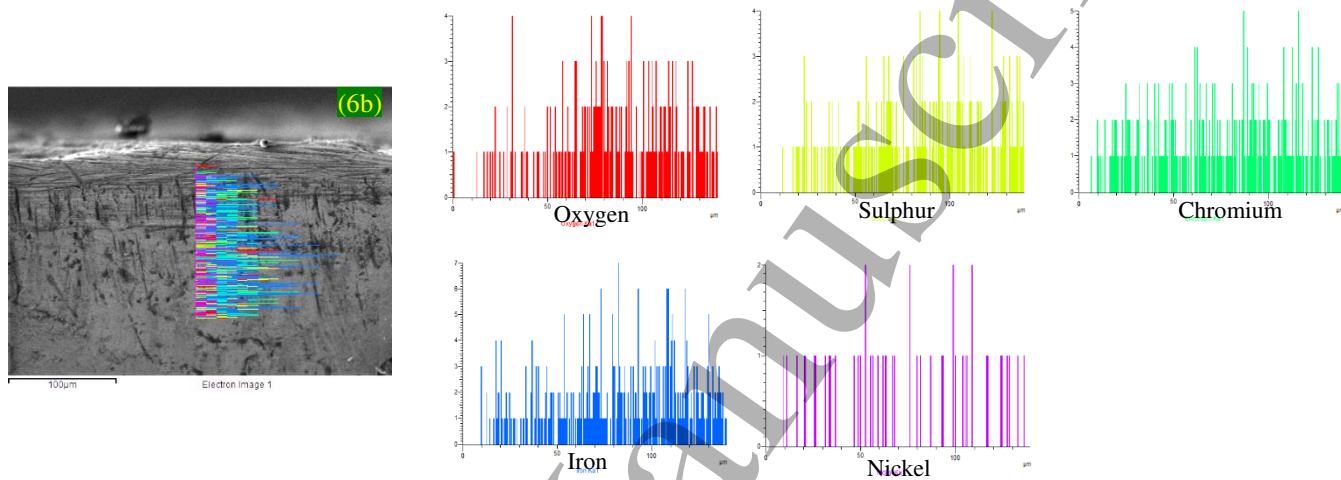


Figure 6b: Cross sectional line mapping images of the specimen exposed to molten salt at 600 °C after 5 cycle.

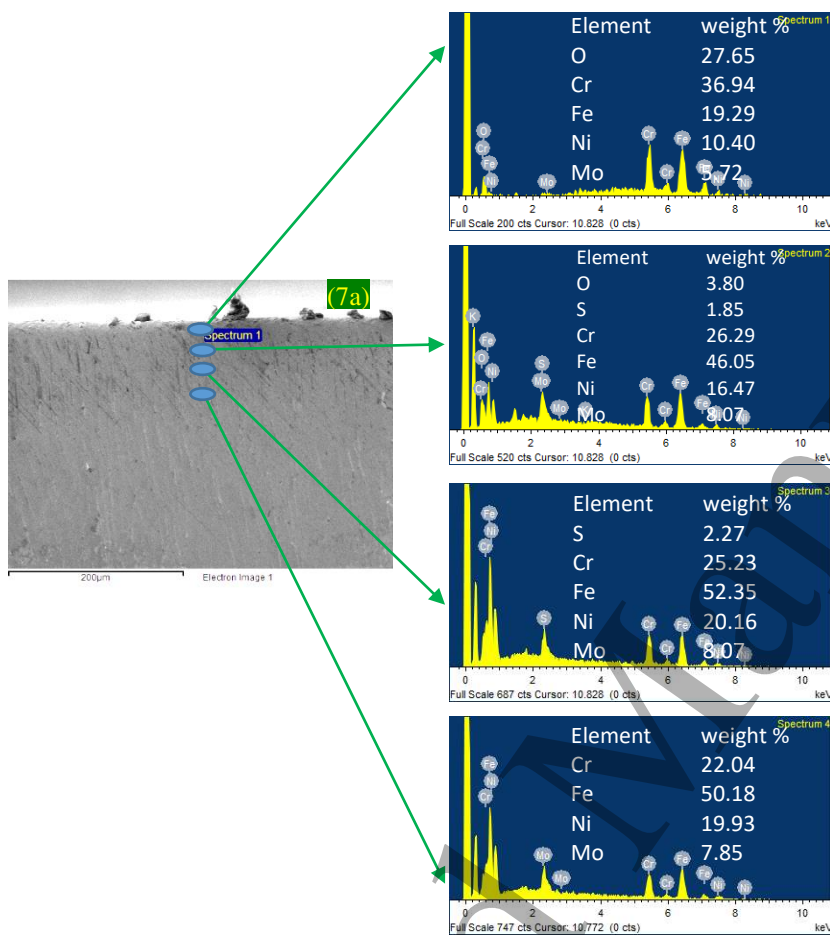


Figure 7a: Cross-sectional SEM images with EDS results of the specimen exposed to air oxidation at 650 °C after 5 cycles.

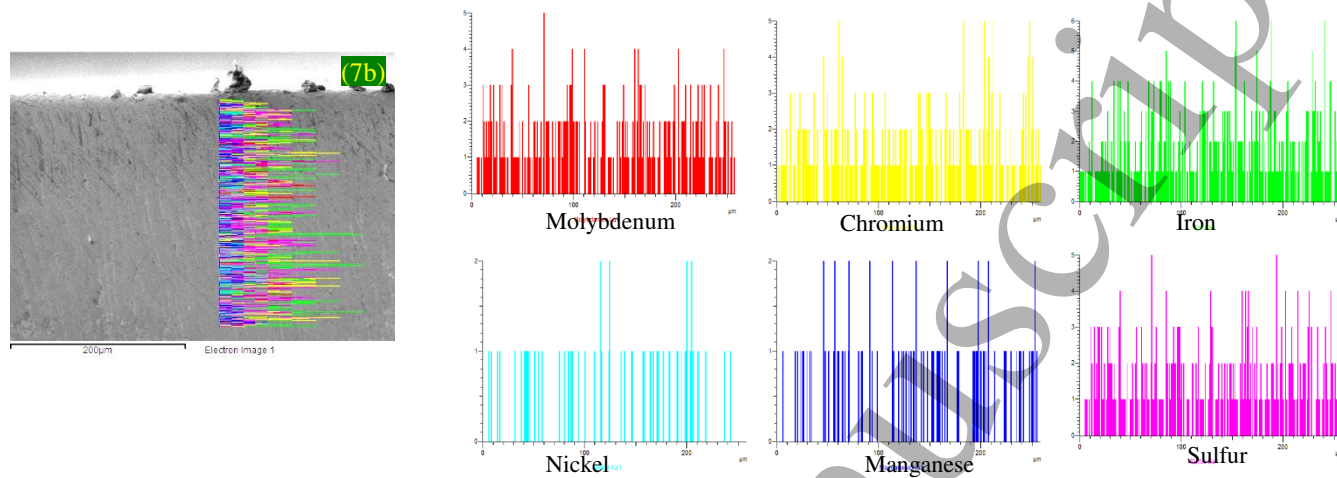


Figure 7b: Cross-sectional line mapping images of the specimen exposed to air oxidation at 650 °C after 5 cycles.

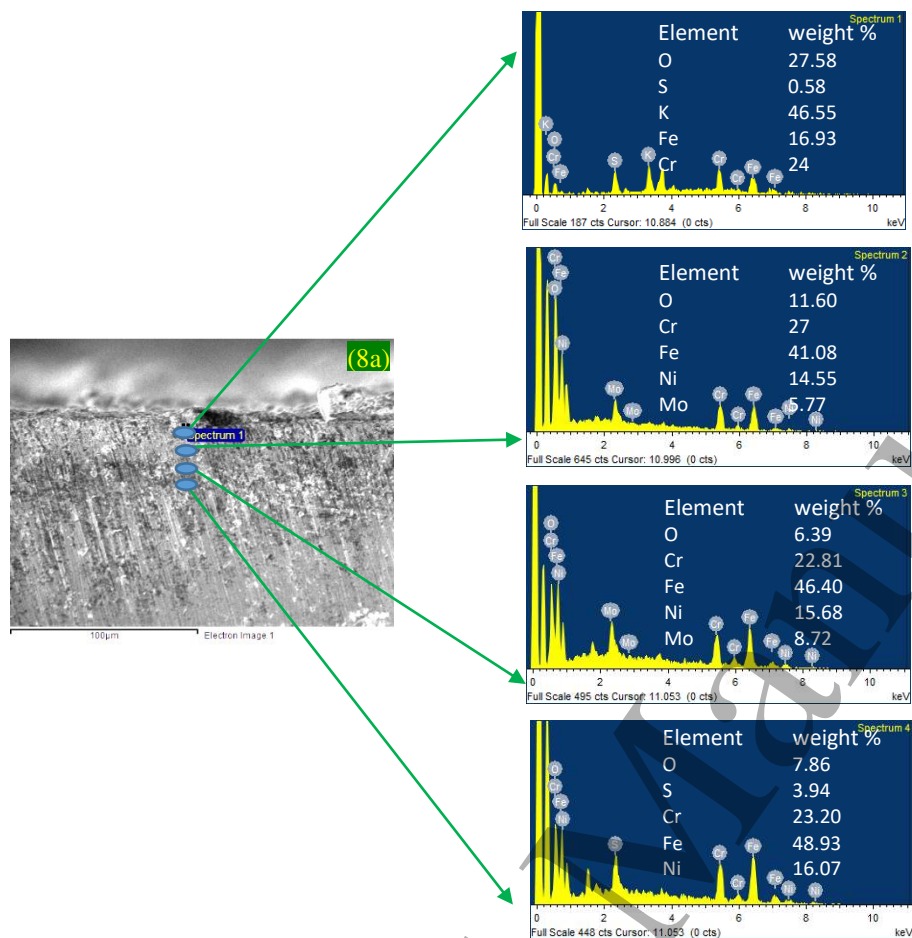


Figure 8a: Cross- sectional SEM images with EDS results of the specimen exposed to molten salt at 650 °C after 5 cycles.

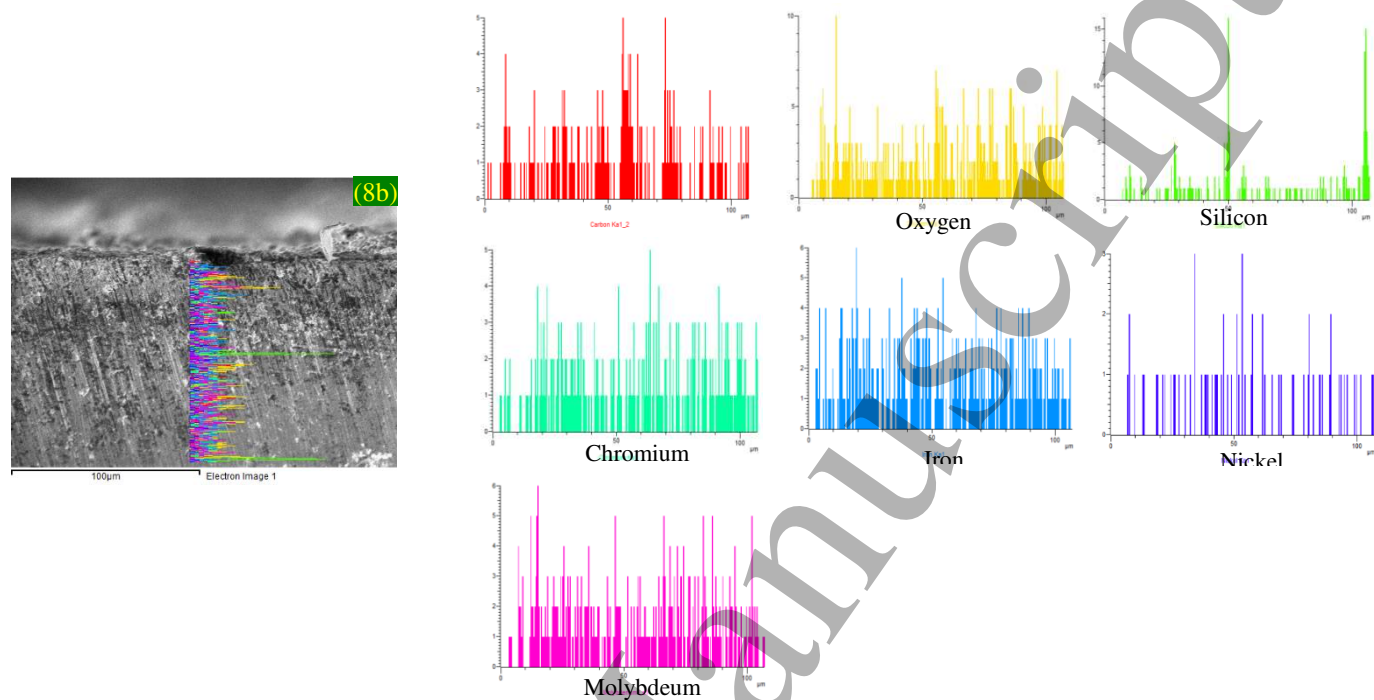


Figure 8b: Cross- sectional line mapping images of the specimen exposed to molten salt at 650 °C after 5 cycles.

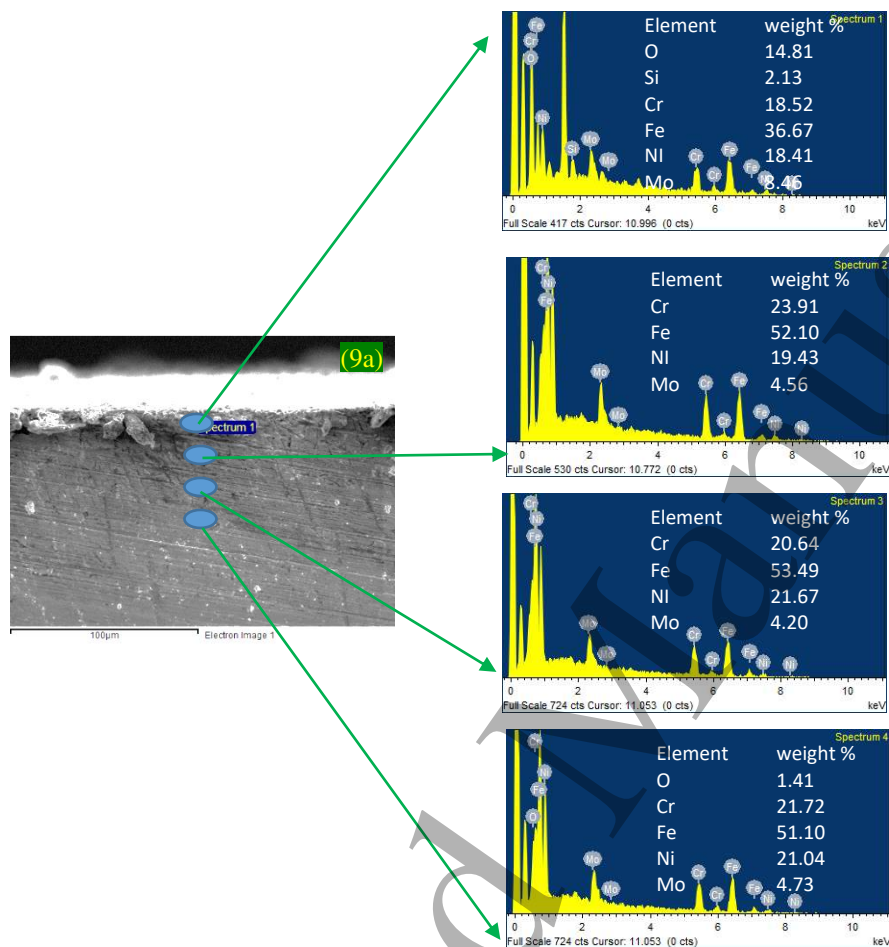
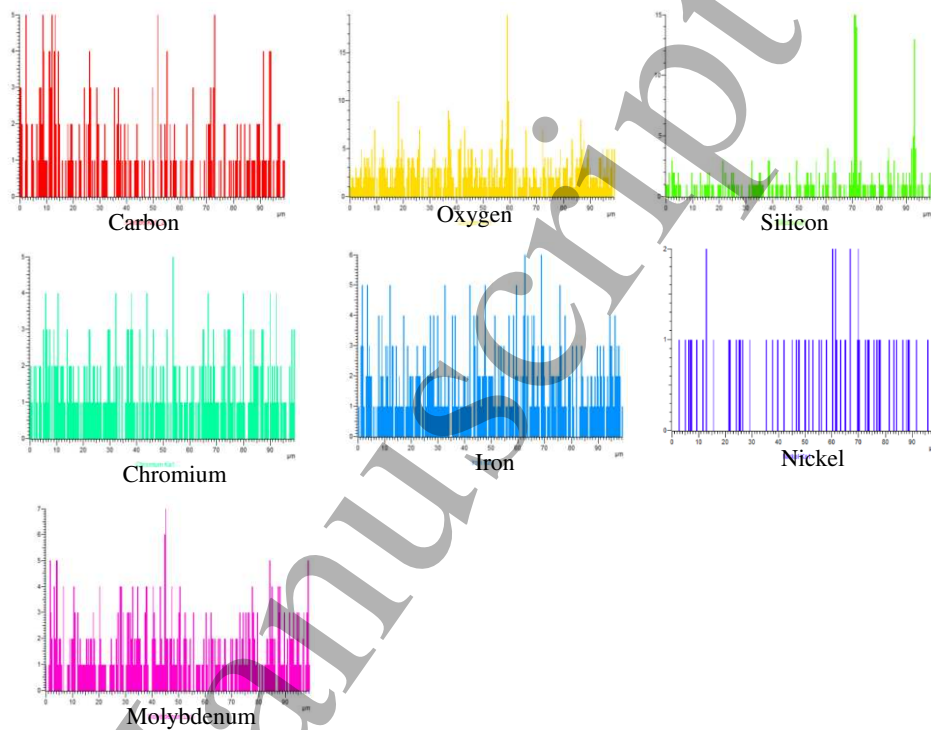
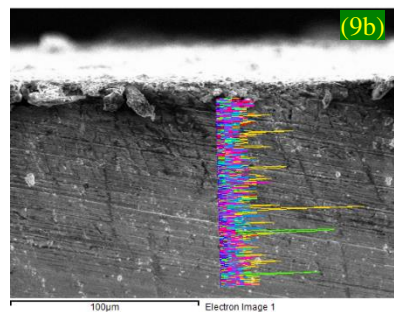


Figure 9a: Cross- sectional SEM images with EDS results of the specimen exposed to air oxidation at 700 °C after 5 cycles.



27 **Figure 9b:** Cross- sectional line mapping images of the specimen exposed to air oxidation at 700 °C after 5
28 cycles.
29
30
31
32
33
34
35
36
37
38
39
40
41
42
43
44
45
46
47
48
49
50
51
52
53
54
55
56
57
58
59
60

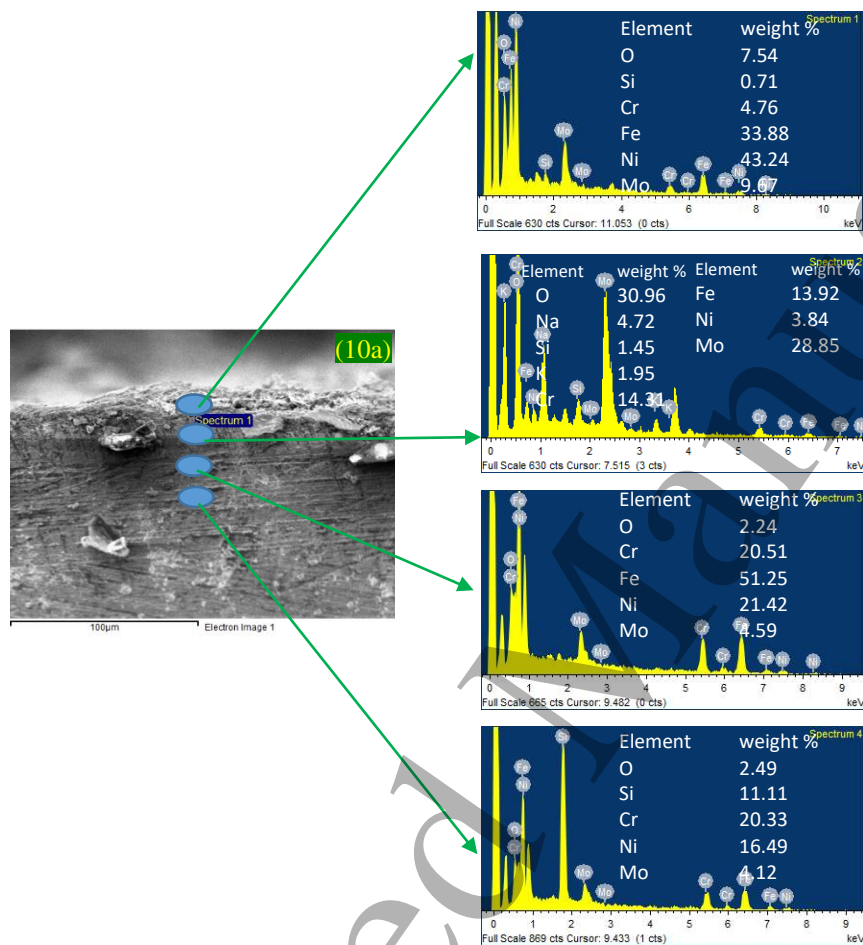
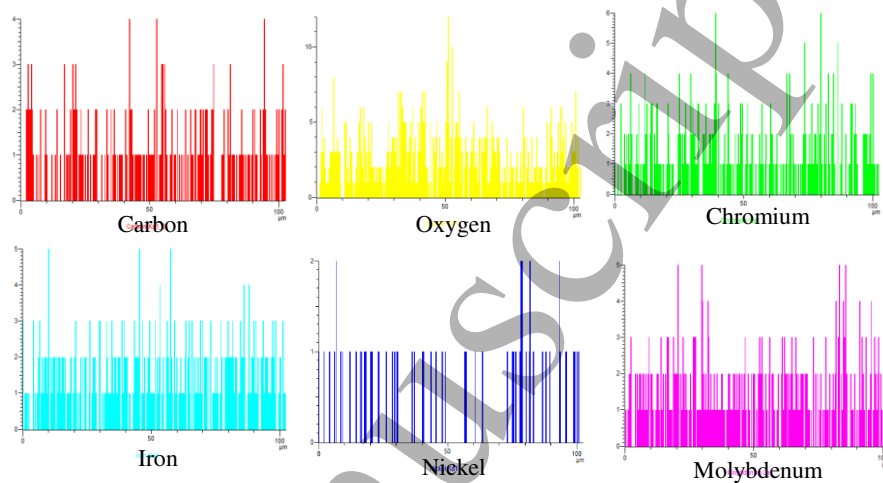
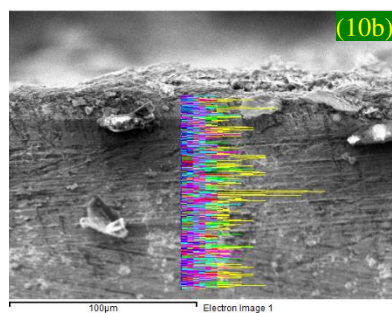


Figure 10a: Cross-sectional SEM images with EDS results of the specimen exposed to molten salt at 700 °C after 5 cycles.



20
21
22
23
24
25
26
27
28
29
30
31
32
33
34
35
36
37
38
39
40
41
42
43
44
45
46
47
48
49
50
51
52
53
54
55
56
57
58
59
60

Figure 10b: Cross-sectional line mapping images of the specimen exposed to molten salt at 700 °C after 5 cycles.

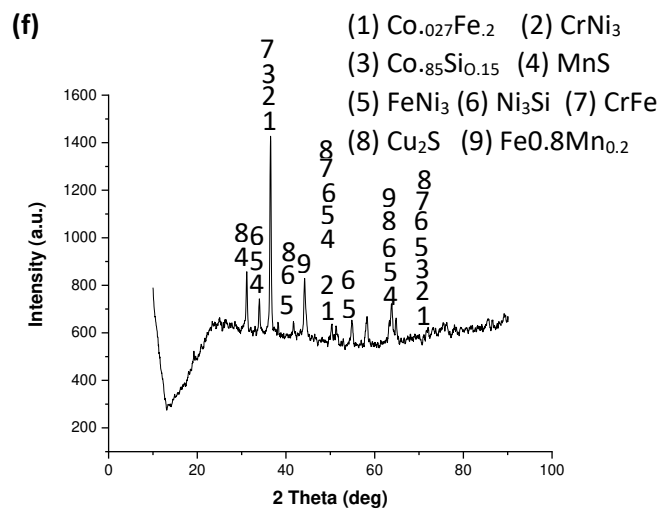
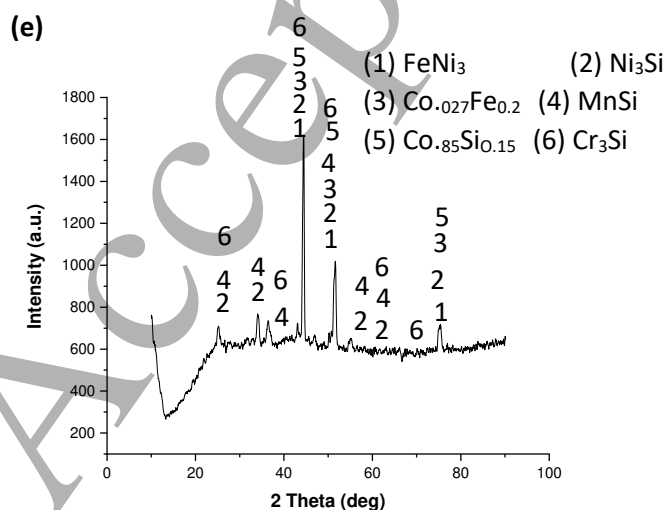
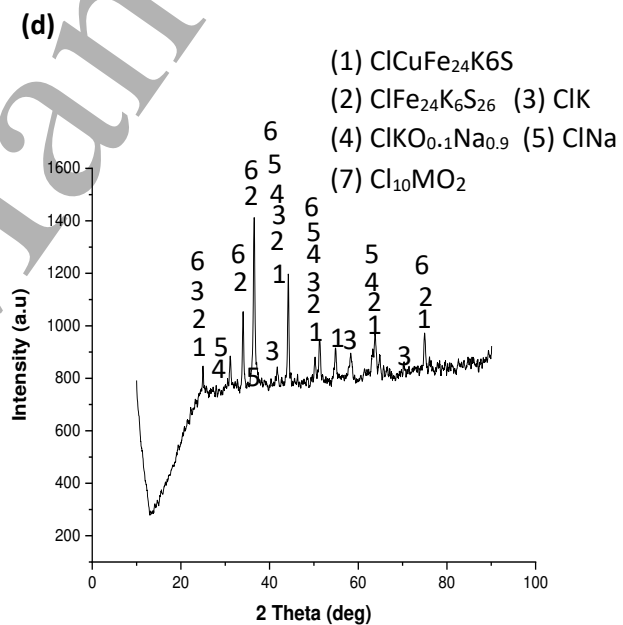
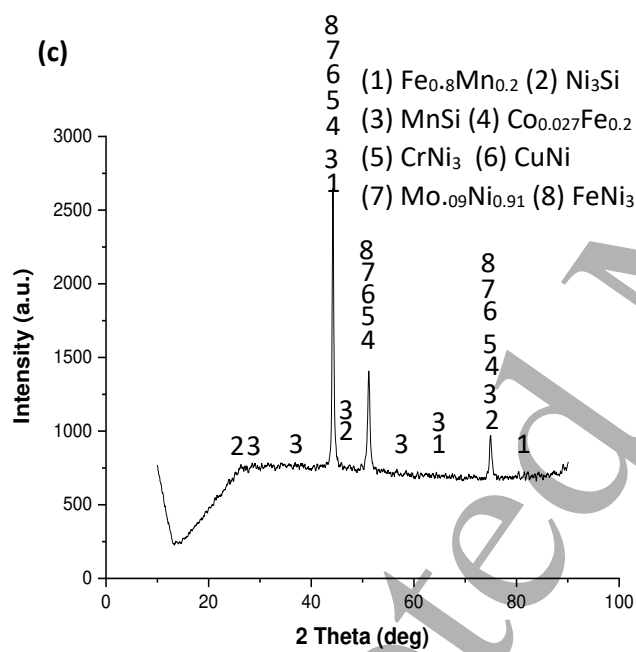
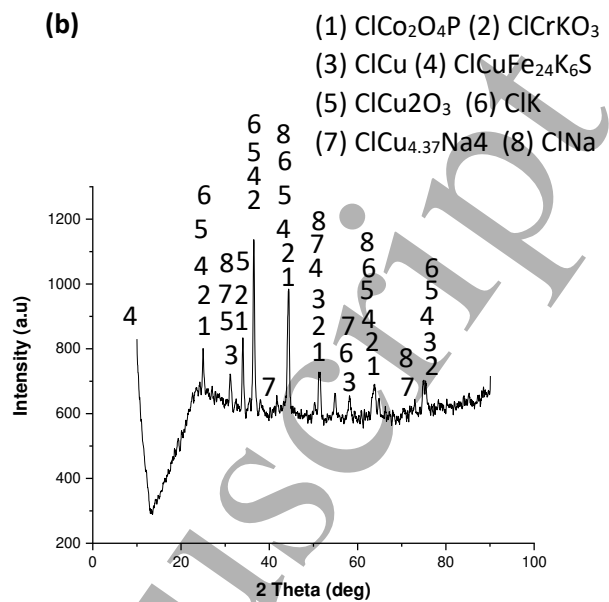
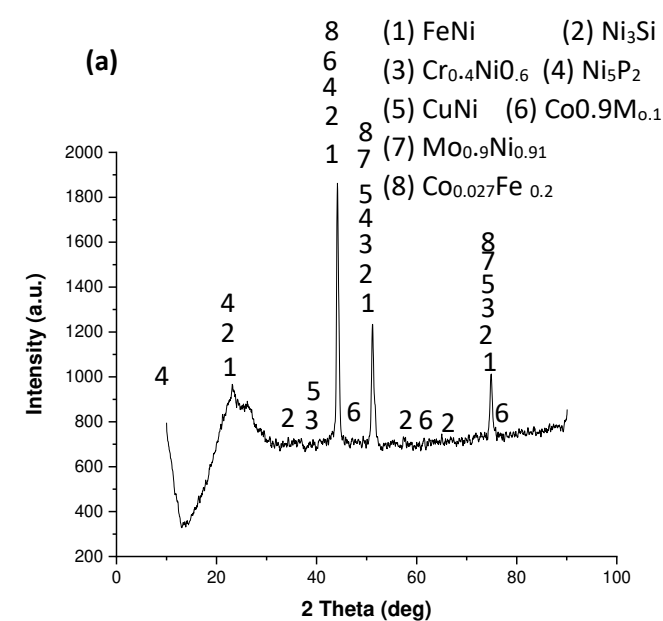


Figure 11: XRD pattern of the specimen after 50 hours of cycle

- (a) specimen after air oxidation at 600 °C (b) specimen after molten salt corrosion at 600 °C
(c) specimen after air oxidation at 650 °C (d) specimen after molten salt corrosion at 650 °C
(e) specimen after air oxidation at 700 °C (f) specimen after molten salt corrosion at 700 °C.

1
2
3
4
5
6
7
8
9
10
11
12
13
14
15
16
17
18
19
20
21
22
23
24
25
26
27
28
29
30
31
32
33
34
35
36
37
38
39
40
41
42
43
44
45
46
47
48
49
50
51
52
53
54
55
56
57
58
59
60

Accepted Manuscript